CrystEngComm

PAPER

View Article Online
View Journal | View Issue

Cite this: *CrystEngComm*, 2015, **17**, 8645

A polar/π model of interactions explains face-to-face stacked quinoid rings: a case study of the crystal of potassium hydrogen chloranilate dihydrate†

Krešimir Molčanov,*[a] Jernej Stare,[b] Biserka Kojić-Prodić,[a] Claude Lecomte,[c] Slimane Dahaoui,[c] Christian Jelsch,*[c] Emmanuel Wenger,[c] Ana Šantić[a] and Bartosz Zarychta[d]

Received 29th May 2015,
Accepted 7th October 2015

DOI: 10.1039/c5ce01037c

www.rsc.org/crystengcomm

The nature of interactions between face-to-face staggered stacked quinoid rings with π-systems, observed with a short inter-ring centroid···centroid distance, is analyzed by experimental and theoretical methods. Charge density studies based on X-ray diffraction and DFT calculations, complemented by impedance spectroscopy, were employed to define the electronic and structural characteristics of the quinoid rings responsible for their interactions within the crystal packing. The crystal packing is mainly stabilized by strong electrostatic interactions between the K^+ cation and the hydrogen chloranilate anion. The proximity and orientation of the stacked quinoid rings in parallel glide-plane arrangement are partly governed by the non-covalent interactions within the dimer. The estimated contribution of dispersion energy to the stacking of the rings about −10 kcal mol^{-1}, as calculated by DFT methods, is comparable to medium–strong hydrogen bonding. The electronic structure of 3,6-dichloro-2,5-dihydroxyquinone monoanion exhibits alternating electron-rich and electron-poor regions. The calculated electrostatic energy shows variations with the relative orientation of rings within dimers reaching *ca.* 10–15 kcal mol^{-1}. Thus, the nature of interactions between π-systems of quinoid rings can be described by a polar/π model where electrostatic complementarity plays a determinant role in π-stacking orientation. These interactions have great potential in crystal engineering and may be employed in the design of functional materials.

Introduction

π-Interactions are a quite common type of intermolecular interaction[1–9] occurring between planar, conjugated π-electron systems and have already found their way into supramolecular chemistry textbooks.[10] However, their exact nature is still a matter of dispute.[5,11–13] π-Interactions are generally considered to be weak, rarely exceeding 2 kcal mol^{-1},[10] but can be considerably enhanced by dipolar interactions.[5,9,14] Nevertheless, they have quite a potential in supramolecular chemistry[15,16] and crystal engineering.[17]

An empirical model for aromatic π-stacking, developed by Hunter and Sanders,[1,6] states that attractive interactions prevail in parallel offset (Fig. 1a) and T-shaped (Fig. 1b) arrangements. Face-to-face eclipsed or alternating arrangements (Fig. 1c and d) are energetically unfavourable for aromatic hydrocarbons due to electrostatic repulsion. However, for arene·perfluoroarene dimers, Salonen *et al.*[12] found by computation that the face-to-face eclipsed $C_6F_6\cdots C_6H_6$ dimer has a negative (*i.e.* attractive) energy and is nearly as favourable as the parallel offset configuration. This is due to the complementary electrostatic potentials between the two molecules.[8] In the current study of a chloranilic acid salt, a new arrangement, parallel non-offset staggered, is found.

Typically in aromatic π–π stacking, distances between ring centroids (and carbon atoms of contiguous rings) are greater than 3.6 Å and greater than the sum of van der Waals radii for carbon, which is 3.5 Å (ref. 18) and offsets are larger than 1.7 Å (about a half of the ring diameter). Such an arrangement observed in the crystal structures[1] is in accordance with *ab initio* calculations[19–21] and suggests that aromatic π-interactions are mainly dispersive interactions with some

[a] *Rudjer Bošković Institute, Bijenička 54, HR-10000 Zagreb, Croatia. E-mail: Kresimir.Molcanov@irb.hr*
[b] *National Institute of Chemistry, Hajdrihova 19, SI-1001 Ljubljana, Slovenia*
[c] *Cristallographie, Résonance Magnetique et Modélisations CNRS, UMR 7036, Institut Jean Barriol, CNRS and Université de Lorraine BP 70239, F54506 Vandoeuvre-les-Nancy CEDEX, France. E-mail: christian.jelsch@univ-lorraine.fr*
[d] *Faculty of Chemistry, Uniwersytet Opolski, Oleska 48, 45-052 Opole, Poland*

† Electronic supplementary information (ESI) available: Details on multipolar refinement, calculations of electrostatic potential and calculated deformation density. CCDC 1403137. For ESI and crystallographic data in CIF or other electronic format see DOI 10.1039/c5ce01037c

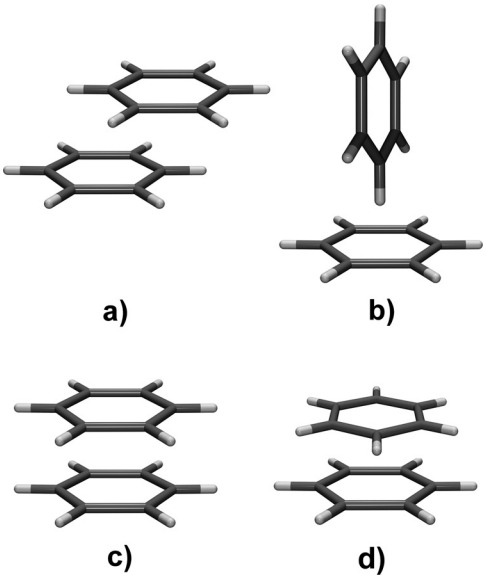

Fig. 1 Possible arrangements of stacked rings: a) parallel-offset and b) T-shaped are energetically favourable for aromatics; less common are parallel, face-to-face, c) eclipsed, and d) staggered.

electrostatic contribution (Fig. 2). In aromatic heterocyclic rings, but not in pure (C,H) compounds, C···C contacts occur frequently in crystal packing as parallel offset π-stacking can be favourable from the electrostatic point of view.[12,22] While the study of π-interactions has been limited almost exclusively to aromatic rings, stacking of other types of planar conjugated rings is neglected.

Quinoid rings (Scheme 1) differ from aromatics due to distinguishable, alternating, single and double bonds.[23] Their different electronic structures imply different types of intermolecular interactions. However, until recently, no attempt has been made to study π-stacking of quinoid rings.

A few years ago, we observed unusual face-to-face stacking in a few alkali salts of a quinoid compound, chloranilic acid (3,6-dichloro-2,5-dihydroxy-*p*-benzoquinone)[24] (Scheme 2), which prompted us to further study the phenomenon. It turned out that alkali salts of various substituted 2,5-dihydroxyquinones tend to form face-to-face stacks,[25–28] in both eclipsed (Fig. 1c)[28] and staggered (Fig. 1d)[24,26,27]

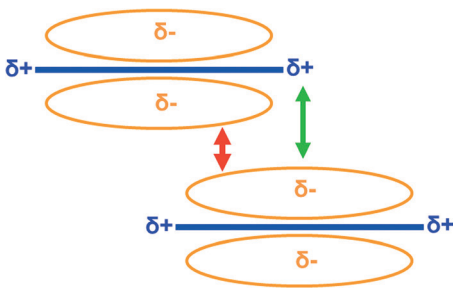

Fig. 2 Interactions between two parallel, offset aromatic rings: the green arrow indicates attraction between electron-poor σ skeleton of one ring and electron-rich π cloud of another, while the red arrow indicates repulsion of π electron clouds (represented by ochre ovals).

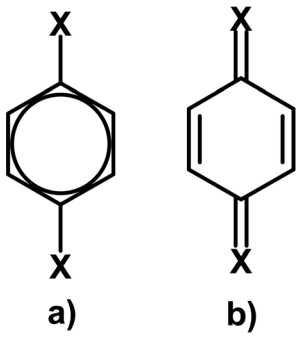

Scheme 1 a) Aromatic and b) quinoid rings.

arrangements. Centroid and interplanar distances in such stacks are about 3.3 Å (0.2 Å shorter than the sum of van der Waals radii for carbon[18]), indicating an unusually strong interaction. Preliminary quantum chemical calculations indicated that these interactions are comparable to hydrogen bonds and are likely stronger than 10 kcal mol^{-1}. Face-to-face alternate arrangement of quinoid rings in the stacks is such to allow a close contact between electron-rich and electron-poor parts of the molecule: electron-rich π-bonds (double and delocalised) are sandwiched between electron-poor σ-bonds and *vice versa* (Fig. 3). Thus, σ–π attractions are maximised, while π–π repulsions are minimised.

Face-to-face staggered π-stacking has been described by Hunter & Sanders[1] (Fig. 1d); it is observed in the crystal packing of 2,3,5,6-tetramethyl-1,4-benzoquinone (duroquinone)[29] and several salts of 3,6-dibromo-2,5-dihydroxyquinone (bromanilic acid).[27] The rotation between two interacting parallel quinones is about 90°.

However, such a simplified model, based exclusively on geometrical data (crystal structures measured with a resolution of 0.8 Å), leaves many questions open. It does not provide an energy estimate of the interaction and says nothing on the possibility of localized charge transfers between two adjacent rings. Due to a close contact between the rings, some degree of reciprocal charge transfer might be possible.

Therefore, we decided to perform a detailed, in-depth study of interactions between face-to-face oriented quinoid rings by using a combination of experimental X-ray charge density, quantum chemical calculations (*ab initio* and periodic DFT), and measurement of electrical properties. As a very convenient model compound, we chose potassium hydrogen chloranilate dihydrate (KHCA·$2H_2O$, Scheme 2).[24] It

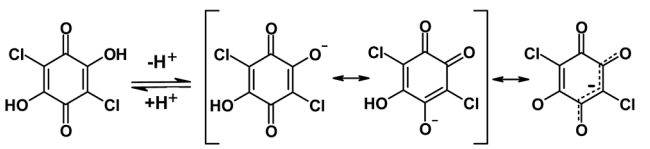

Scheme 2 Dissociation of chloranilic acid to the monoanion with resonance structures shown in brackets. The monoanion comprises single, double and delocalised C–C and C–O bonds.

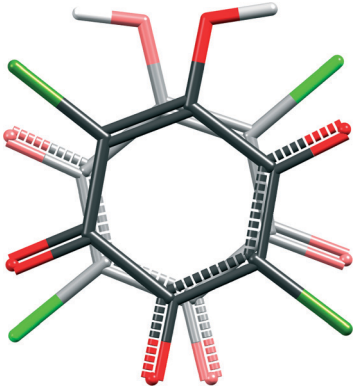

Fig. 3 A simplified representation of face-to-face alternate (staggered) arrangement of hydrogen chloranilate anions related by a glide-plane: electron-rich π-bonds (double and delocalised) are sandwiched between electron-poor σ-bonds (single). Atoms are colour-coded: C, black/dark gray; O, red; Cl, green; H, light gray.

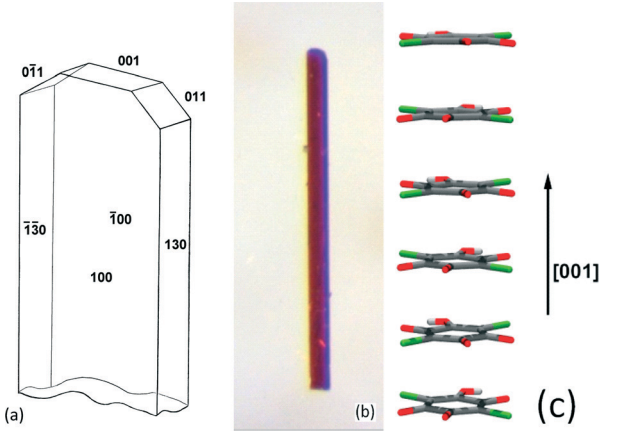

Fig. 4 a) The crystal habit of KHCA·2H_2O with combinations of crystal forms; the {011} form is developed just exceptionally, b) photograph of the real sample (the crystal is 0.8 mm long), and c) perspective view of a face-to-face arrangement of hydrogen chloranilate anions in KHCA·2H_2O.

is very stable and easy to prepare, grows into large well-developed crystals and comprises only light atoms, which do not introduce a problem of large X-ray absorption.

Results and discussion

To gain insight into the nature of the face-to-face interaction (Table 1), X-ray charge density analysis was assisted by DFT calculations utilizing periodic and isolated cluster models, revealing the role of non-bonding interactions and the energetics of stacking. A possible reciprocal charge transfer between the rings was probed by impedance spectroscopy. A detailed study of crystal morphology is required for both charge density determination (to correct absorption) and impedance spectroscopy (to apply electrical contacts at specific faces), but it also gives some insight into the dominant interactions in the crystal.

Crystal morphology

Crystals of KHCA·2H_2O, $P2_1/c$, are needle-like, elongated in the direction of the c axis, which is also the direction of ring stacking between equidistant (3.17 Å) hydrogen chloranilate anions (Fig. 4). The largest and best developed forms are {100}, and the crystals are very thin in the direction of the a axis. This implies that they grow rapidly in the [001] direction but very slowly in the [100] direction. Therefore, we can expect that the strongest intermolecular interactions are parallel to the c axis and the weakest ones are parallel to the a axis. Indeed, the crystal packing comprises layers of cations, anions and water molecules linked together by cation⋯anion interactions and hydrogen bonds; these layers are parallel to the (100) plane (Fig. 5 and Table 2). They are linked by only two symmetry-independent hydrogen bonds (Table 2). Therefore, we should expect that the strong interaction in the [001] direction is mainly due to the K^+/anion interactions linking two adjacent quinoid rings and secondarily due to the face-to-face staggered arrangement of the rings. The potassium coordination is made up of five chlorine and two oxygen atoms. On the other hand, there are two hydrogen bonds approximately perpendicular to the c axis and one approximately parallel to it (Table 2).

Table 1 Geometric parameters defining π⋯π stacking arrangements between two adjacent rings C1 → C6 ⋯C1 → C6

Plane distance (Å)	3.1746(2)
Cg⋯Cg′ distance (Å)	3.176(3)
Cg⋯Cg′ offset (Å)	0.087
α angle between the ring planes (°)	0.00
β angle between the Cg⋯Cg′ line and normal to the planes (°)	1.58
Dihedral angle C6–Cg–Cg′–C12′ (°)	101

Symmetry operator on Cg′ and O3′: x, 3/2 − y, −1/2 + z.

Electronic structure of the hydrogen chloranilate anion based on X-ray charge density studies and DFT calculations

The experimental deformation electron density of the hydrogen chloranilate anion (Fig. 6a) is in good agreement with

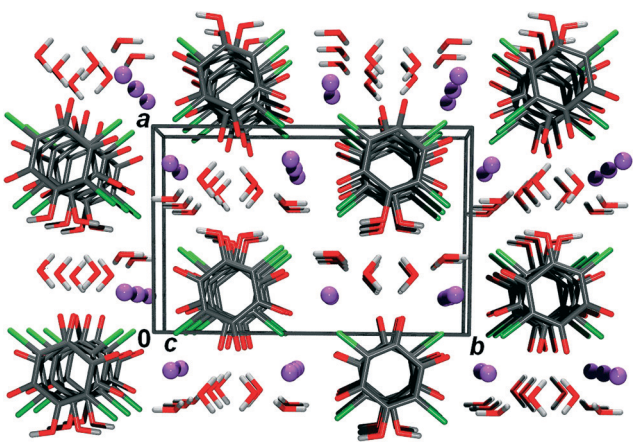

Fig. 5 Crystal packing of KHCA·2H_2O viewed approximately along the [001] direction. Potassium cations (in violet) are shown as spheres of arbitrary radii.

Table 2 Geometric parameters of hydrogen bonds

	d(D–H)/Å	d(H···A)/Å	d(D···A)/Å	D–H···A/°	Symm. operator on A
O1–H1···O5	0.967(2)	1.827(2)	2.613(3)	136.4(6)	$-1+x, 3/2-y, -1/2+z$
O5–H5A···O6	0.967(2)	1.811(2)	2.758(2)	165.3(3)	$x, y, 1+z$
O5–H5B···O2	0.967(2)	2.026(3)	2.835(3)	140.1(6)	$-x, 1/2+y, 1/2-z$
O6–H6A···O3	0.967(2)	1.870(2)	2.835(3)	176.53(6)	$x, 3/2-y, -1/2+z$
O6–H6B···O1	0.967(2)	1.993(2)	2.954(3)	173.2(1)	$1+x, y, z$

the simplified structural formula (Scheme 2) derived from molecular geometry.[24] It is a very interesting system for studying covalent bonds since this relatively small anion comprises three types of C–C and C–O bonds: formally single, formally double and delocalised (bond order of about 1.5). Table 3 gives the topological properties of all covalent bonds as calculated from multipolar refinement against experimental and theoretical intensities; the agreement between experiment and theory is very good. We note an overall larger charge density at CPs for the experimental one. According to this topological analysis, C–C bonds can indeed be classified into these three types. Formally single bonds, C1–C2, C4–C5 and C5–C6, have the lowest electron density at the critical point and are the least elliptical. We note that both experimental and theoretical C5–C6 ellipticities are larger than 0.2; the C5–C6 bond is also shorter compared to typical C–C single bonds (1.51–1.54 Å) in the Engh & Huber dictionary[30] and has considerably higher electron density at the CP than typical single C–C bonds; therefore, it is more similar to delocalised bonds. The shortest formal single bond C5–C6 can be regarded as an elongated delocalised bond. Therefore, its bond order is quite greater than 1. The formally double bond, C6═C1, has the largest electron density ρ_{cp} value but is also longer than usual (d = 1.34 Å (ref. 31)) and its ellipticity is lower than the 0.45 value found in double bonds;[32] therefore, its bond order is lower than two.

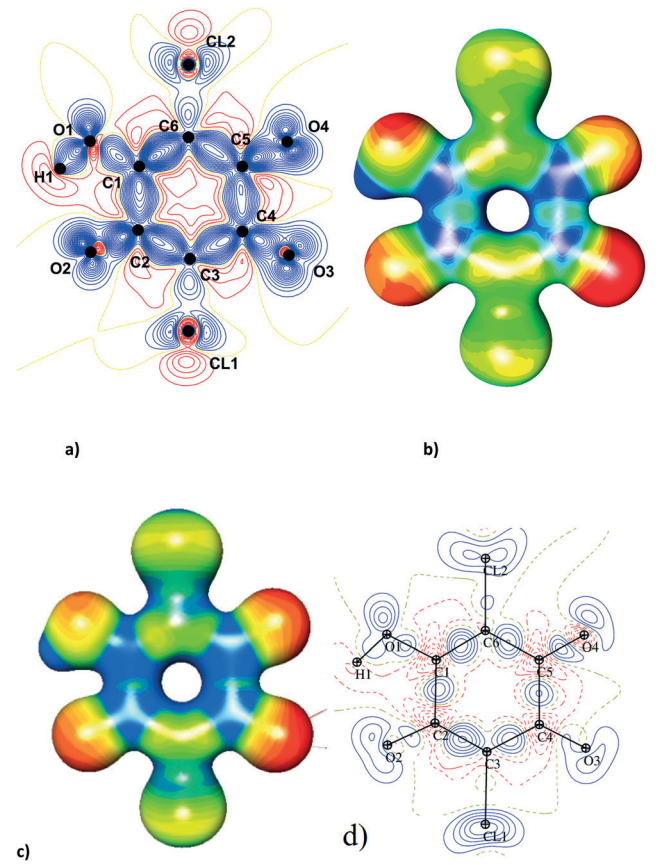

Fig. 6 a) Experimental deformation density of the hydrogen chloranilate anion. Positive density is shown in blue and negative density in red; yellow dotted lines represent zero density. Contours are drawn for 0.05 e Å^{-3}. b) Multipolar experimental and c) theoretical electrostatic potentials mapped on an electron density isosurface of 0.35 e Å^{-3}. Colour scale −0.25 to +0.3 e Å^{-1}. d) The same as a) but at an elevation of 0.5 Å above the ring plane.

Topological properties of delocalized C–O bonds (Table 3) are very close to those of a C═O bond, and the formally single bond, C1–O1, is 0.06 Å shorter than similar C–O bonds in hydroquinones.[33,34] It is also interesting to note that C–Cl bonds have much lower ρ_{cp} electron density (in agreement with ref. 35) than either C–O or C–C bonds,[8] which can easily be noted in the deformation density map (Fig. 6a). Experimental and theoretical multipolar electrostatic potentials (as calculated from ref. 36) (Fig. 6b and c) are also in excellent agreement with the simple delocalisation model (Scheme 2).

Most of the negative potential is located around O atoms as expected; the electrostatic potential around the chlorine atoms is less electronegative as already observed.[35] Atom O4, which is formally neutral, is a weaker attractor than O2 and O3. In the carbon skeleton, alternating electropositive and electronegative regions are observed: a negative electrostatic potential can be found in the regions of double and delocalised bonds and positive about the single C–C bonds. This experimental picture supports our previous simple model (Scheme 2 and Fig. 3)[24] and is in very good agreement with the quantum chemical calculations. The uneven distribution of electropositive and negative potentials in the quinoid ring plays an important role in the stacking interactions, as shown below.

Anion···anion interactions as revealed by charge density analysis

Since KHCA·2H_2O is an ionic compound, the strongest and the most important interactions in the crystal packing are of ionic nature. Cation···anion interactions therefore provide the "scaffolding", and more subtle details of the crystal packing are governed by weaker intermolecular interactions. We

Table 3 Topology of C–C and C–O bonds derived from experimental and *CRYSTAL09* computation electron density after multipolar refinement. Bond C5–C6 is listed as formally single; however, according to electron density, it is more similar to delocalised bonds

Formal bond		Length (Å)		Electron density rho (CP) (e Å^{-3})		Laplacian (e Å^{-3})		Ellipticity	
		Exp	Theo	Exp	Theo	Exp	Theo	Exp	Theo
Single	C1–C2	1.5059(17)	1.5138	1.7904	1.7110	−13.2	−12.0	0.16	0.17
	C4–C5	1.5419(17)	1.5456	1.6387	1.6253	−10.5	−10.5	0.19	0.15
	C5–C6	1.4551(16)	1.4539	1.9438	1.8690	−14.9	−13.9	0.22	0.23
Delocalized	C2–C3	1.4095(16)	1.4143	2.1372	2.0166	−19.1	−16.0	0.31	0.30
	C3–C4	1.4068(15)	1.4118	2.0895	2.0200	−18.4	−16.0	0.28	0.29
Double	C6═C1	1.3577(15)	1.3666	2.2984	2.2171	−22.4	−17.6	0.35	0.37
Single	C1–O1	1.3182(15)	1.2960	2.3379	2.1604	−23.3	−19.4	0.05	0.07
Delocalized	C2–O2	1.2450(14)	1.2482	2.8422	2.5874	−34.9	−24.5	0.10	0.08
	C4–O3	1.2430(14)	1.2467	2.7293	2.5867	−28.9	−24.5	0.07	0.07
Double	C5═O4	1.2227(14)	1.2285	2.8987	2.7299	−33.8	−23.7	0.15	0.07

have studied quite a few alkali salts of chloranilic acid[24–26] and its analogues,[27,28] which are sterically similar; however, face-to-face stacking occurs only in some of them. Dianions form offset, aromatic-like stacks,[24–27] while in the case of monoanions, stacking is sometimes offset[24] but, more commonly, face-to-face. While the steric effect of the cation certainly influences stacking, π-interactions between the rings should be regarded as important also. However, since hydrogen chloranilate moieties are anions, strong repulsions between them should occur, compensated by cation···anion attractions.[37a] The charge distribution in the chloranilate anion is such that most of the negative potential is located in the outer region of the anion oxygen atoms (Fig. 6b and c and Table S1 in the ESI†), which form close contacts with potassium cations (Fig. 5). The face-to-face arrangement of anions in the stacks then minimises electrostatic repulsions while maximising any dispersive attractive interactions. This novel type of stacking and the fine-tuning of the interactions between quinoid rings are a major topic of this work. As we will show, it is the result of the peculiarly uneven distribution of electron density in the carbon ring that leads to electropositive and electronegative regions.

The charge density analysis of these stacked anions in a face-to-face arrangement (Fig. 7a) reveals that the close contacts between the rings always involve an electron-rich area of one ring and an electron-poor area of another ring. Therefore, electrostatic repulsion between two stacking anions is considerably attenuated.

Topological analysis of the electron density reveals the bond paths linking the atoms in contact and the critical points (CPs, Fig. 8). There are three saddle CPs between carbon atoms of contiguous rings with an electron density maximum of around 0.058 e Å^{-3} (Table 4 and Fig. 8) and four other saddle CPs between the substituent O and Cl atoms similar to those observed in the non-centrosymmetric phase of the TTF–CA charge transfer complex[8] (Table 4). In addition, a (3,+3) critical point is found between the rings, indicating the centre of the cage.

Table 4 gives the experimental and theoretical topological properties of the electron density at the critical points within a pair of hydrogen chlorinate anions. The agreement between experiment and theory is very good. There are three saddle critical points between carbon atoms of contiguous rings (C3···C5, C5···C3, C2···C6) and four other saddle points

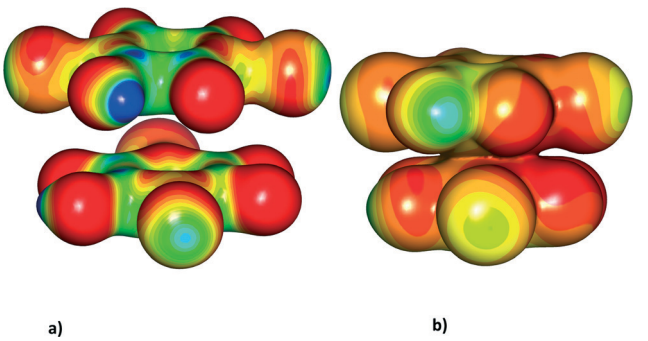

Fig. 7 Multipolar experimental electrostatic potential of a pair of contiguous hydrogen chloranilate rings a) mapped on an isosurface of 0.35 e Å^{-3} showing interactions between electron-rich (red and orange) and electron-poor (blue, green) regions and b) mapped on an isosurface of 0.05 e Å^{-3} showing electron density between carbon skeletons. Scale: a) −0.35 to +0.35; b) −0.6 to +0.2 e Å^{-1}.

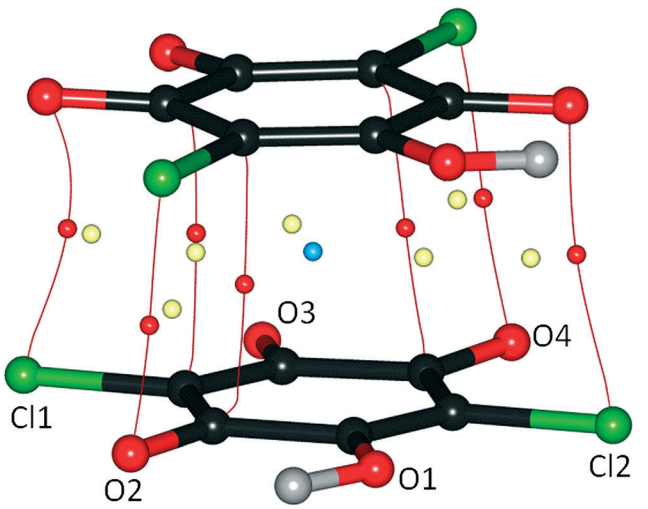

Fig. 8 Critical points in a π-stack. (3,–1) CPs and their bond paths are shown in red, (3,+1) ring CPs are shown in yellow and the (3,+3) cage CP is shown in blue.

Table 4 Electron density (ρ_{tot}) and Laplacian values at the critical points within a pair of hydrogen chloranilate anions

		ρ_{tot}		Lapl.		G_{cp}	V_{cp}
A···B	Distance	Exp	Theo	Exp	Theo	Exp	Exp
C3···C5	3.212(3)	0.059	0.049	0.61	0.55	3.3	−2.7
C5···C3	3.236(3)	0.057		0.58		3.2	−2.5
C6···C2	3.210(3)	0.058	0.051	0.60	0.57	3.3	−2.6
O4···Cl1	3.405(3)	0.039	0.045	0.49	0.61	2.5	−1.7
Cl2···O2	3.351(3)	0.038	0.044	0.55	0.60	2.7	−1.8
Cl1···O4	3.287(3)	0.046	0.039	0.62	0.51	3.1	−2.2
O2···Cl2	3.322(3)	0.046	0.040	0.59	0.56	3.0	−2.2
Cage CP		0.027	0.021	0.29	0.26		

Symmetry operator on atom A: x, $3/2 - y$, $-1/2 + z$.

between the O and Cl substituents. The average experimental electron density and Laplacian at C···C critical points are 0.054 e A^{-3} and +0.58 e A^{-5}, respectively. This closed shell interaction is in line with a weak electrostatic interaction occurring between C3···C5 and C2···C3 carbon atoms as shown by their Bader charges of opposite signs (Table 7). Concerning the Cl···O interactions, their positive Laplacian shows their closed shell nature while the negative charge of all Cl and O atoms is in favour of a dispersive character of the interaction which counteracts the electrostatic repulsion. The $|V|/G$ ratios lower than unity (Table 4) confirm the closed shell interaction of all C···C and Cl···O contacts. It allows the use of the Abramov[37b] approximation to estimate the interaction energy *via* the formula $E_{dissoc} \approx -V/2$ proposed by Espinosa *et al.*[37c] As expected from their closest shell character, these interaction energies are small around 1 kcal mol^{-1}; the stabilizing interaction energy sum of the dimer in its crystal environment can then be estimated as 7 kcal mol^{-1} by adding the six C···C and O···Cl interactions.[37d]

The electrical conductivity measurements using a single crystal sample (Fig. 11 and experimental section) suggest that there is no reciprocal electron transfer between the adjacent rings. The electrical conductivity along the c axis is 2.1×10^{-11} $(\Omega\ cm)^{-1}$ at room temperature indicating insulating characteristics of the sample.

The electrostatic energy between two anions using the experimental multipolar atom model is repulsive (+65.7 kcal mol^{-1}). However, when only the six carbon atoms of the ring are considered, the electrostatic interaction energy E_{elec} = −6.4 kcal mol^{-1} is indeed attractive (see Table 5). Therefore, two adjacent C_6 rings are in attractive electrostatic interaction, where electron-deficient regions are facing electron-rich parts of the moiety. The alternance of electron-rich and electron-poor regions is highlighted in Fig. 6d, showing the deformation electron density at an elevation of 0.5 Å above the plane. In addition, there are differences within the C atoms and also within the C–C bonds, due to the different bond orders and atom substituents. The charge of atoms is given with different definitions in Table 7. The P_{val} derived charges are not considered as the best defined charges, as some charge transfer occurs also between bonded atoms in the Hansen & Coppens model through the multipoles. The

Table 5 Electrostatic energy calculated from experimental charge density

Interaction	E_{elec}/kcal mol^{-1}	Symmetry operator on the second group
$HCA^-\cdots HCA^-$	+65.7	
$HCA^-\cdots HCA^-$ def(NEU)[b]	+8.7	
$HCA^-\cdots HCA^-$ multipolar	+2.0	x, $3/2 - y$, $-1/2 + z$
C_6 ring$\cdots C_6$ ring[a]	−6.4	
$HCA^-K^+\cdots HCA^-K^+$	+29.6	
$K + \cdots HCA^-$	−49.8	x, y, z
$K^+\cdots HCA^-$	−42.4	$-x$, $1/2 + y$, $1/2 - z$
$K^+\cdots HCA^-$	−30.3	x, $-y + 3/2$, $z + 1/2$
$K^+\cdots HCA^-$	−30.2	$x - 1$, y, z
$K^+\cdots HCA^-$	−21.4	$-x$, $2 - y$, $-z$
$K^+\cdots HCA^-$	−7.5	x, $-y + 3/2$, $z + 1/2$

[a] Only C_6 core of the ring, without substituents. [b] Integration of (deformation density × deformation potential) after global neutralization of HCA^- anions.

Bader charges integrated with atomic basins, the fitted charges, as well as the P_{val} charges are negative for the chlorine and oxygen atoms on the organic cation.

This is consistent with the simplified model (Fig. 3). On the other hand, the O and Cl atom substituents around the carbon ring do not form a favourable electrostatic interaction within a dimer of HCA^- even if the anion global charge is neutralized or if only the multipolar electron density is taken into account (Table 5). This can be explained by the systematic electron accumulation found on the four oxygen atoms and the two chlorine atoms above and below the ring plane, as illustrated in Fig. 6d.

The electron density between the two rings can be inspected in Fig. 7. Between carbon skeletons, electron density exceeds 0.05 e $Å^{-3}$ (Fig. 7b and Table 4), which is similar to what is observed for some non-covalent attractive interactions.[8] Despite the global electrostatic repulsion of two stacking anions, the distance between two parallel HCA^- planes is only 3.17 Å (Table 1). It should also be noted that the electron density between substituted atoms around the ring does not reach values as high as in the inner carbon region (Fig. 7a and b). This can be attributed to the angle offset between the two C6 rings which has more effect on the periphery.

The dipole moment of the anion (computed for a neutralized ring) has an amplitude of 7.5 D and is directed from the ring centre towards the OH group (Fig. S6 in the ESI†). As can be deduced from Fig. 3, the dipole moments of two contiguous rings are far from being oppositely directed. Therefore, the optimization of the ring orientation has to be analysed using the whole multipolar development and in the more global context of the electrostatic forces in the crystal packing while the van der Waals energy also needs to be taken into account.

Stacking of hydrogen chloranilate anions in view of DFT calculations

In order to elucidate the nature of interactions governing the stacking of the HCA^- quinoid rings and their proximity, we

performed DFT calculations on dimers, by (approximately) excluding or including dispersion interactions. Due to constraints imposed by the size of the system, the DFT approach appears to be the method of choice. While clearly advantageous by fully supporting periodicity, many 'traditional' DFT methods, such as B3LYP or PBE, are notorious for their lack of dispersion and, consequently, poor description of non-bonding interactions. Fortunately, recent development of DFT methodologies facilitates the inclusion of dispersion corrections in various forms. In such a way, DFT methods offer good compromise between accuracy and affordability even when non-covalent interactions represent a crucial factor for the structure of crystalline solids.

In this work, we employed a comparative treatment of a selected model, by using DFT without and with dispersion corrections. The role of non-covalent interactions may be qualitatively deduced by comparing the results of the two. For both isolated and periodic DFT, as implemented in Gaussian and VASP, the Grimme DFT-D2 correction can be simply toggled on or off. We used a similar comparative strategy in our previous investigations of the stacked quinoid rings, yielding reasonable results.[28]

Periodic calculations. Starting from the experimental crystal structure data, we performed full optimization of the system, including atomic positions and unit cell parameters. Table 6 lists the optimized unit cell parameters obtained by either using or omitting the DFT-D2 dispersion correction.

There is a steady trend of shrinking of the unit cell on including the dispersion correction, which is clear evidence that non-covalent, dispersive forces play a significant role in the structure of the system. The dispersion-included approach yields clearly better agreement with the experimental structure for the above listed parameters. This is in agreement with the findings published in our previous work.[28] By far, the largest difference between the dispersion-included and dispersion-omitted methods is in the value of the unit cell constant *c*. Inclusion of dispersion reduces the value of *c* by no less than 0.434 Å, and the dispersion-corrected methodology provides significantly better agreement with the experiment. Since the HCA^- rings stack along the cell vector *c* and the stacking distance is equal to half the length of parameter *c*, this provides strong evidence that, among the structural motifs of the present system, the dispersion and/or dipolar interaction components between the rings most significantly influence the stacking proximity.

Gas phase calculations. We further investigated the role of non-bonding interactions on a stacked dimer model of two HCA^- rings. Fig. 9 displays the interaction energy of two rings as a function of their torsional alignment, calculated by the PBE functional with and without the DFT-D2 dispersion correction.

Table 6 Optimized unit cell parameters and volume of $KHCA{\cdot}2H_2O$ calculated without and with the DFT-D2 dispersion corrections of the PBE functional. Experimental values are listed as reference

	Dispersion off	Dispersion on	Experimental
a [Å]	10.051	9.889	9.986(9)
b [Å]	15.338	15.308	15.210(16)
c [Å]	6.647	6.213	6.350(5)
β [°]	100.04	98.86	99.09(3)
V [Å^3]	1009	929	952(2)

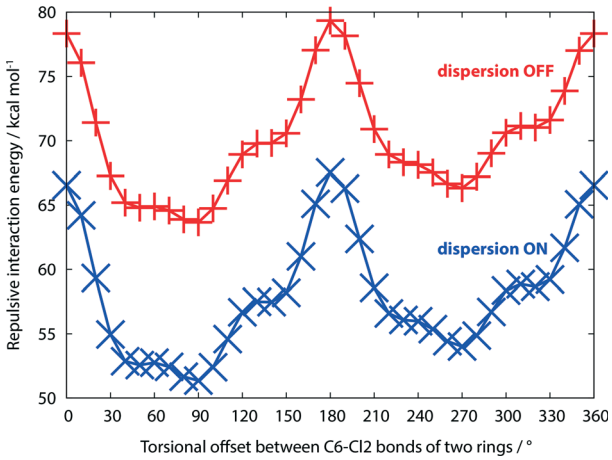

Fig. 9 Counterpoise-corrected pairwise interaction energy of a pair of stacked HCA^- rings, computed with the PBE functional with and without the DFT-D2 dispersion correction and the 6-311++G(2d,2p) basis set, as a function of their torsional alignment (see Fig. 10).

Both profiles exhibit significant repulsion originating from the fact that each ring bears a negative charge (Table 7). The profiles are nearly identical, spanning a range of about 10 kcal mol^{-1} from lowest to highest repulsion. Remarkably, the experimental torsional alignment of about 101° (expressed as torsional offset between the C6–Cl2 bonds, see Fig. 10) is very close to the global 90° minimum of both profiles. This confirms that the alignment of the rings follows the tendency of minimizing electrostatic repulsion and also supports the aforementioned

Table 7 Atomic charges (*e*). P_{val} derived values are from the $Q = N_{val} - P_{val}$ difference between number of valence electrons in neutral and refined multipolar atoms. Esd's were obtained after refinement *vs.* all variables. Fitted charges were obtained with VMoPro software from the electrostatic potential in a 0.1 Å thick layer around the van der Waals surface

Atom	X-ray P_{val} derived	X-ray Bader	X-ray fitted	Theoretical P_{val} derived
K1	+1.00[a]	+0.97		+0.91(4)
Cl1	−0.09(3)	−0.53	−0.071	−0.08(1)
Cl2	−0.22(3)	−0.68	−0.180	−0.12(1)
O1	−0.27(6)	−1.06	−0.465	−0.32(1)
H1	+0.33(6)	0.64	0.397	+0.30(1)
O2	−0.17(5)	−0.93	−0.424	−0.30(1)
O3	−0.33(4)	−1.01	−0.610	−0.28(1)
O4	−0.14(4)	−0.96	−0.336	−0.20(1)
C1	+0.07(7)	0.46	0.228	−0.01(3)
C2	−0.10(9)	0.70	0.254	+0.05(3)
C3	−0.23(7)	−0.11	−0.458	+0.06(3)
C4	+0.16(7)	0.79	0.661	+0.05(3)
C5	−0.01(8)	0.85	0.010	+0.02(3)
C6	−0.13(7)	−0.03	−0.171	+0.08(3)
Correlations	X-ray P_{val}	0.756	0.879	0.756
	X-ray Bader		0.845	0.838
	X-ray fitted			0.715

[a] Constrained to unity.

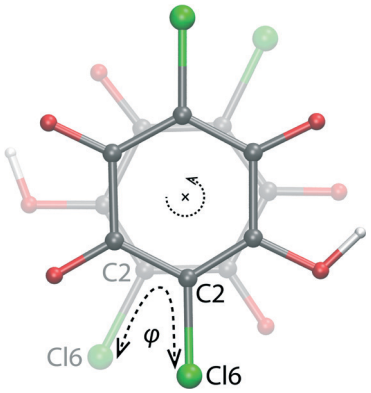

Fig. 10 Model for the calculation of orientation-dependent interaction energy of a stacked pair of hydrogen chloranilate ions (the displayed case corresponds to φ = 30°).

view that the overlap between the electron-rich and electron-poor domains of the neighbouring rings provides substantial stabilization. The electrostatic energy derived from the experimental charge density is actually very similar to the energy value obtained by B3LYP calculation (Table 5 and Fig. 10).

The ~12 kcal mol^{-1} shift between the profiles demonstrates significantly lower repulsion derived from the functional improved for the dispersion interactions. We believe that a significant part of this difference can be attributed to the non-covalent interaction between the rings. Although quantitative determination of the π-interaction component is beyond the reach of the present study, it can be safely assumed that its amount is substantial. The computed difference in interaction energy due to dispersion correction is nearly twice as large as found in our previous study of a system of stacked di-anion quinoid rings (~7 kcal mol^{-1}),[28] which is likely to be attributed to the closer stacking distance (by more than 0.3 Å) in the present case.

Conclusions

This paper presents a detailed study of an unusual type of face-to-face stacking, as a contribution to the development of a more general theory of stacking of planar π-systems. Substituted quinones have revealed quite often face-to-face arranged quinoid rings[24–27] with a separation distance significantly shorter than the sum of carbon···carbon van der Waals radii. Their stacking motifs and geometrical parameters are different to those observed for aromatic rings. The recent theoretical papers,[11,13,19,38–40] which discuss the nature of interactions between aromatic rings, came to the conclusion that 'π-stacking' and 'π···π-interactions' do not accurately describe the forces responsible for association of aromatics. A more plausible explanation is that the aromatic π-interactions are dispersive, coupled by weak electrostatic interactions between electron-rich and electron-poor moieties. For some aromatic systems, notably T-shaped interactions, the π-electron-rich cloud of one ring and the electron-poor σ-electron skeleton of another ring form favourable electrostatic interactions. These interactions, such as $C^{\delta-}\cdots H^{\delta+}$ contacts occurring in aromatic hydrocarbons, have been called σ–π attractions.

In heterocycles, substituted with electronegative atoms such as oxygen and halogens, π-stacking with translational and/or rotational offset happens more frequently. The presence of both electro-positive and negative moieties within the aromatic planar groups enables the formation of stacks with a good electrostatic complementarity.[12,22]

Such a concept which is valid for aromatics can be generalized to other π-systems, including quinoid rings. In the system studied, potassium hydrogen chloranilate dihydrate, quinoid rings in the stacks are equidistant, with an interplanar separation of 3.176(3) Å and a negligible translation offset of only 0.087 Å (compared to more than 1.6 Å in aromatic stacks).

Two adjacent C_6-rings appear staggered, with a rotation of 11°. While ionic interactions are dominant in the crystal packing, face-to-face staggered stacking is in addition directed by more subtle electrostatic interactions between the quinoid rings' delocalised systems. The dispersion energy of stacking interaction was estimated by quantum chemical calculations to be about −10 to −15 kcal mol^{-1}, which is one order of magnitude stronger than better-known aromatic π-interactions. The dispersion energy does not appear to be dependent on the relative orientation of the rings.

Conversely, significant variations reaching 10 kcal mol^{-1} are observed for the electrostatic energy, due to a better complementarity occurring in favourable orientations (Fig. 9). When the electrostatic interaction energy of a stacking HCA^- dimer is computed *in vacuo*, the most favourable orientation (90°) corresponds to a perfectly staggered C_6 ring dimer. Due to several strong ionic bridges between the HCA^- substituent atoms and surrounding K^+ cations, the equilibrium orientation is shifted by 11° and occurs at 101° in the crystal packing.

Our findings on the nature of interactions between π-systems of quinoid rings are in line with the most recent papers[8,13,19,38–40] which consider a combination of dispersion and favourable electrostatic attractions rather than specialised π···π interactions. Such electrostatic attraction model is realistic and can be applied to all heterocyclic molecules having π-systems (not only to aromatics).

Experimental

X-ray diffraction and multipolar refinement

The crystals were prepared as reported previously.[24] The morphology of the crystals was studied using a Unicam optical goniometer. X-ray diffraction measurements were performed using a Bruker D8 Venture diffractometer at 100 K. The full Ewald sphere was measured with the maximum resolution of 0.50 Å. The program package Bruker Apex[41] was used for data reduction and analytical absorption correction. The multiple integrated reflections were averaged for the space group $P2_1/c$ using SORTAV[42] adapted to area detector data. The spherical-atom model was refined using SHELXL-97;[43] atomic coordinates were taken from the room-temperature structure.[24]

For multipolar refinement (*vs.* F^2), the program package MoPro[44] was used. Anisotropic parameters for hydrogen atoms were calculated by the SHADE server[45] and imported into the multipolar model (and constrained during the refinement); O–H distances were restrained to 0.967(2) Å. Since the two water molecules have higher thermal motion, constraints had to be applied on the charge density. The four water H atoms were set to be chemically equivalent as well as their two O atoms. Potassium cation was refined as a monopole. Wenger[46] in his PhD thesis showed that high resolution scale factors are accurate and constant over the resolution range only when a pixel hybrid detector is used contrary to CCD or CMOS data. Then, as these data are CMOS data, a polynomial scale factor as a function of $s = \sin\theta/\lambda$ was derived:

$$I_{obs} = I_{calc} \times k(1 + \alpha_2 s^2 + \alpha_3 s^3)$$

Such a correction which is available in MoPro[43] leads to significant reduction of residual electron density around the potassium atom.

Geometry, charge-density and electrostatic property calculations were performed using MoPro;[44] molecular graphics were prepared using MoProViewer[47] and ORTEP-3.[48] The exact electrostatic energy calculation was performed according to the EP/MM method described by Coppens *et al.*[49] Crystallographic and refinement data for KHCA·2H_2O are shown in Table 8; additional details on refinement are deposited as ESI.†

Table 8 Crystallographic, data collection and experimental charge-density refinement details

Compound	KHCA·2H_2O
Empirical formula	$C_6H_5Cl_2KO_6$
Formula wt/g mol^{-1}	283.096
Crystal dimensions/mm	0.415 × 0.052 × 0.031
Space group	$P2_1/c$
a/Å	9.986(9)
b/Å	15.210(16)
c/Å	6.350(5)
α/°	90
β/°	99.09(3)
γ/°	90
Z	4
V/Å^3	952(2)
D_{calc}/g cm^{-3}	1.975
μ/mm^{-1}	1.123
$\sin\Theta/\lambda$	1.0182
T/K	100(2)
Radiation wavelength	0.71073 (MoKα)
Diffractometer type	Bruker D8 Venture
Range of h, k, l	$-20 < h < 20$; $-30 < k < 30$; $-12 < l < 12$
Reflections collected	179 543
Independent reflections	7923
Observed reflections ($I \geq 2\sigma$)	5688
Absorption correction	Analytical
T_{min}, T_{max}	0.725, 0.972
Weighting scheme	$w = 1/[0.13^*/s^2(F_o^2)]$
R_{int}	0.0432
R (F)	0.0132
R_w (F^2)	0.0263
Goodness of fit	0.554
H atom treatment	Restrained, anisotropic
No. of parameters	397
No. of restraints	5
$\Delta\rho_{max}$, $\Delta\rho_{min}$ (e Å^{-3})	0.672; −0.467

Quantum chemical calculations

Both periodic and isolated models were considered. Periodic calculations were performed by using the program package *VASP v. 5.2*,[50] including full geometry optimization of the crystal structure (atomic positions and cell parameters). The PBE functional[51] was used together with a plane-wave basis set with a cutoff of 500 eV and the projector augmented wave atomic pseudopotentials.[52] A sufficiently dense 3 × 2 × 5 k-point mesh was employed. Optimization was performed both without and with the addition of the Grimme DFT-D2 dispersion correction[53] to the original PBE functional. Symmetry constraints of the $P2_1/c$ space group were followed during optimization.

The gas phase calculations were performed by using the *Gaussian 09* program suite.[54] The model consisted of a pair of stacked hydrogen chloranilate rings extracted from the experimental crystal structure. By rotating the rings along the line passing through their centres perpendicularly to the plane of the rings (Fig. 10), their pair interaction energy was calculated for each configuration by the PBE functional with included or omitted DFT-D2 dispersion corrections, in conjunction with the 6-311++G(2d,2p) basis set.[55–57] The interaction energies were corrected for basis set superposition errors by using the counterpoise method. During the scan, the internal structure (bond lengths and valence angles) of the chloranilate anions was fixed to the experimental geometry. For practical reasons, the rings were made planar, which was the only (very subtle) modification of the experimental data.

Theoretical charge density

Periodic quantum mechanical calculations using *CRYSTAL09* (ref. 58) were performed at the crystal geometry observed experimentally, and using this as a starting geometry, optimization was performed with density functional theory (DFT) method[59] and with the *B3LYP* hybrid functional[60] using 6-31G(d,p) basis set.[61] For the potassium atom, the triple-zeta valence with polarization basis set developed by Peintinger *et al.*[62] was used.

Upon convergence on energy (ΔE ~ 10^{-6} hartree), the periodic wave function based on the optimized geometry was obtained. The coordinates of hydrogen atoms were relaxed, but the unit cell was kept fixed. The index generation scheme proposed by Le Page & Gabe[63] was applied to generate Miller indices up to s = 1.2 Å^{-1} reciprocal resolutions. The option *XFAC* of the *CRYSTAL09* program was then used to generate a set of theoretical structure factors from the computed electron density and using a set of prepared indices. The theoretical charge density was refined *vs.* all the generated structure factor amplitudes.

Theoretical multipolar refinement

The multipolar refinement based on the theoretical structure factors $F(hkl)$ was performed using all reflections up to resolution d = 0.42 Å. The atomic positions were fixed to the values obtained from the geometry relaxation, the scale factor was fixed to unity and atomic thermal motion parameters were set to zero. The valence and multipole populations and kappa coefficients were refined together with block-diagonal option in several cycles until convergence. Neither restraints nor constraints were imposed to the electron density distribution of the atoms, except for the H atoms, for which the parameters were restrained to a value of 1.16(1).

Measurement of electrical conductivity

Electrical conductivity of the single crystal sample along the crystallographic c axis was measured by impedance spectroscopy (Novocontrol Alpha-N dielectric analyser) in the frequency range of 0.01 Hz–1 MHz at room temperature. For the electrical contacts, silver paint electrodes (rectangular, 0.417 mm × 0.083 mm) were deposited on the opposite surfaces (*i.e.* {001} faces) of the crystal. The impedance spectrum was analysed by equivalent circuit modelling using the complex nonlinear least-squares fitting procedure (*ZView* software).

The complex impedance plot of the single crystal exhibits an arc with high values of impedance indicating low electrical conductivity (Fig. 11).

The experimental impedance data can be approximated by the equivalent circuit consisting of a parallel combination of a resistor and a capacitor. The parameters of the equivalent circuit, *i.e.* electrical resistance (R) and capacitance (C), obtained by the complex non-linear least squares fitting are listed in Fig. 11. From the values of electrical resistance (R) and electrode dimensions (A is the electrode area and d is the sample thickness), DC conductivity is calculated according to the relation $\sigma_{DC} = d/(A \cdot R)$. The electrical conductivity of the single crystal sample at room temperature is equal to 2.1×10^{-11} $(\Omega\ \mathrm{cm})^{-1}$.

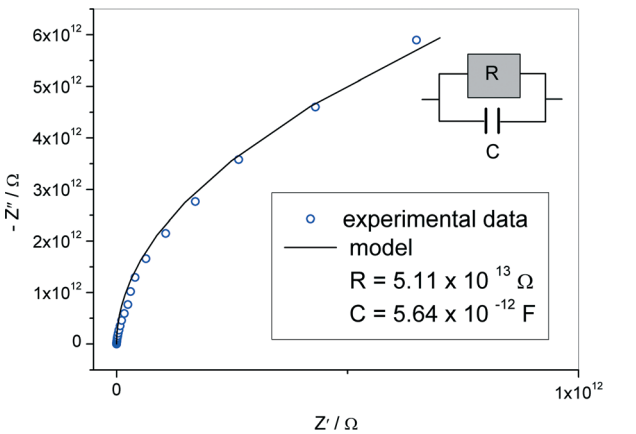

Fig. 11 Complex impedance plot and the corresponding equivalent circuit.

Acknowledgements

The financial support from the Ministry of Science, Education and Sports of the Republic of Croatia (Slovenian-Croatian bilateral collaboration grant for years 2012–2013), French-Croatian bilateral – Hubert Curien grant for years 2015–2016, the Croatian Academy of Sciences and Arts (for 2014), Croatian Science Foundation (grant no. IP-2014-09-4079) and Slovenian Research Agency (grant no. P1-0012) is gratefully acknowledged. K. M. is grateful to a joint RBI/French Embassy scholarship for a visit to Nancy. Diffraction measurements were performed at the Institut Jean Barriol X-ray diffraction facility. We thank Dr. Robert Vianello, RBI, Zagreb, Croatia, for performing the gas phase DFT calculations with DFT-D2 dispersion corrections by using Gaussian 09.

Notes and references

1 C. A. Hunter and J. K. M. Sanders, *J. Am. Chem. Soc.*, 1990, **112**, 5525–5534.
2 C. A. Hunter, *Angew. Chem., Int. Ed. Engl.*, 1993, **32**, 1584–1586.
3 C. A. Hunter, *Chem. Soc. Rev.*, 1994, **23**, 101–109.
4 M. L. Głowka, D. Martynowski and K. Kozłovska, *J. Mol. Struct.*, 1999, **474**, 81–89.
5 C. Janiak, *J. Chem. Soc., Dalton Trans.*, 2000, 3885–3896.
6 C. A. Hunter, K. R. Lawson, J. Perkins and C. J. Urch, *J. Chem. Soc., Perkin Trans. 2*, 2001, 651–659.
7 E. A. Mayer, R. K. Castellano and F. Diedrich, *Angew. Chem., Int. Ed.*, 2003, **42**, 1210–1250.
8 P. García, S. Dahaoui, C. Katan, M. Souhassou and C. Lecomte, *Faraday Discuss.*, 2007, **135**, 217–235.
9 S. E. Wheeler, *Acc. Chem. Res.*, 2013, **46**, 1029–1038.
10 J. W. Steed and J. L. Atwood, *Supramolecular Chemistry*, J. Wiley & Sons, Chichester, U.K., 2nd edn, 2009; H. Krause, B. Ernstberger and H. J. Neusser, *Chem. Phys. Lett.*, 1991, **184**, 411–417; J. R. Grover, E. A. Walters and E. T. Hui, *J. Phys. Chem.*, 1987, **91**, 3233–3237; S. Tsuzuki, K. Honda, T. Uchimaru, M. Mikami and K. Tanabe, *J. Am. Chem. Soc.*, 2002, **124**, 104–112.
11 S. Grimme, *Angew. Chem., Int. Ed.*, 2008, **47**, 3430–3434.
12 L. M. Salonen, M. Ellermann and F. Diedrich, *Angew. Chem., Int. Ed.*, 2011, **50**, 4808–4842.
13 C. R. Martinez and B. L. Iverson, *Chem. Sci.*, 2012, **3**, 2191–2201.
14 K. Molčanov and B. Kojić-Prodić, *CrystEngComm*, 2010, **12**, 925–939.
15 M. W. Hosseini, *Acc. Chem. Res.*, 2005, **38**, 313–323.
16 F. J. M. Hoeben, P. Jonkheim, E. W. Meijer and A. P. H. J. Schenning, *Chem. Rev.*, 2005, **105**, 1491–1546.
17 J. K. Klosterman, Y. Yamauchi and M. Fujita, *Chem. Soc. Rev.*, 2009, **38**, 1714–1725.
18 B. Cordero, V. Gómez, A. E. Platero-Prats, M. Revés, J. Echeverría, E. Cremades, F. Barragán and S. Alvares, *Dalton Trans.*, 2008, 2832–2838.
19 E. C. Lee, D. Kim, P. Jurečka, P. Tarakeshwar, P. Hobza and K. S. Kim, *J. Phys. Chem. A*, 2007, **111**, 3446–3457.

20 M. O. Sinnokrot and D. C. Sherril, *J. Phys. Chem. A*, 2006, **110**, 10656–10668.
21 Y. C. Park and J. S. Lee, *J. Phys. Chem. A*, 2006, **110**, 5091–5095.
22 C. Jelsch, K. Ejsmont and L. Huder, *IUCrJ*, 2014, **1**, 119–128.
23 S. Hünig, *Pure Appl. Chem.*, 1990, **62**, 395–406.
24 K. Molčanov, B. Kojić-Prodić and A. Meden, *CrystEngComm*, 2009, **11**, 1407–1415.
25 K. Molčanov, B. Kojić-Prodić and A. Meden, *Croat. Chem. Acta*, 2009, **82**, 387–396.
26 K. Molčanov, B. Kojić-Prodić and I. Sabljić, *CrystEngComm*, 2011, **13**, 4211–4217.
27 K. Molčanov and B. Kojić-Prodić, *Acta Crystallogr., Sect. B: Struct. Sci.*, 2012, **68**, 57–65.
28 K. Molčanov, B. Kojić-Prodić, D. Babić and J. Stare, *CrystEngComm*, 2013, **15**, 135–143.
29 R. Shukla and R. Rathore, *Synthesis*, 2008, 3769–3774.
30 R. A. Engh and R. Huber, *Acta Crystallogr., Sect. A: Found. Crystallogr.*, 1991, **47**, 392–400.
31 M. A. Fox and J. K. Whitesell, *Organische Chemie, Grundlagen, Mechanismen, Bioorganische Anwendungen*, Springer, 1995.
32 D. Stalke, *Chem. – Eur. J.*, 2011, **17**, 9264–9278.
33 K. Molčanov, B. Kojić-Prodić and M. Roboz, *Acta Crystallogr., Sect. B: Struct. Sci.*, 2006, **62**, 1051–1060.
34 K. Molčanov, B. Kojić-Prodić, D. Babić, D. Žilić and B. Rakvin, *CrystEngComm*, 2011, **13**, 5170–5178.
35 T. T. T. Bui, S. Dahaoui, C. Lecomte, G. R. Desiraju and E. Espinosa, *Angew. Chem., Int. Ed.*, 2009, **48**, 3838–3841.
36 N. Ghermani, C. Lecomte and N. Bouhmaida, *Z. Naturforsch., A: Phys., Phys. Chem., Kosmophys.*, 1983, **48**, 91–98; N. E. Ghermani, N. Bouhmaida and C. Lecomte, *Acta Crystallogr., Sect. A: Found. Crystallogr.*, 1993, **49**, 781–789; N. E. Ghermani, N. Bouhmaida, C. Lecomte and A. Thalal, *Acta Crystallogr., Sect. A: Found. Crystallogr.*, 1997, **53**, 556–563; N. E. Ghermani, N. Bouhmaida, C. Lecomte and A. Thalal, *Acta Crystallogr., Sect. A: Found. Crystallogr.*, 1999, **55**, 729–738.
37 (*a*) C. Lecomte, E. Espinosa and C. F. Matta, *IUCrJ*, 2015, **2**, 161–163; (*b*) Y. A. Abramov, *Acta Crystallogr., Sect. A: Found. Crystallogr.*, 1997, **53**, 264–272; (*c*) E. Espinosa, E. Molins and E. Lecomte, *IUCrJ*, 1998, **285**, 170–173; (*d*) M. E. Brezgunova, J. Lieffrig, E. Aubert, S. Dahaoui, P. Fertey, J. G. Ángyán, M. Formigué and E. Espinosa, *Cryst. Growth Des.*, 2013, **13**, 3283–3289.
38 P. Munshi and T. N. Guru Row, *Crystallogr. Rev.*, 2005, **11**, 199–241.
39 A. Coskun, J. Spruell, G. Barin, A. Fahrenbach, R. Forgan, M. Colvin, R. Carmieli, D. Benítez, E. Tkatchouk, D. Friedman, W. A. Goddard III and J. Stoddart, *J. Am. Chem. Soc.*, 2011, **133**, 4538–4547.
40 J. Spruell, A. Coskun, D. Friedman, R. Forgan, A. Sarjeant, A. Trabolsi, A. Fahrenbach, G. Barin, W. Paxton and S. Dey, *Nat. Chem.*, 2010, **2**, 870–879.
41 *APEX2, SADABS and SAINT*, Bruker AXS Inc., Madison, Wisconsin, USA, 2010.
42 R. H. Blessing, *Crystallogr. Rev.*, 1987, **1**, 3–58.
43 G. M. Sheldrick, *Acta Crystallogr., Sect. A: Found. Crystallogr.*, 2008, **64**, 112–122.
44 C. Jelsch, B. Guillot, A. Lagoutte and C. Lecomte, *J. Appl. Crystallogr.*, 2005, **38**, 38–54.
45 A. Madsen, *J. Appl. Crystallogr.*, 2006, **39**, 757–758.
46 (*a*) E. Wenger, *PhD thesis*, Université de Lorraine, May 2015; (*b*) E. Wenger, P. Allé, S. Dahaoui, D. Schaniel and C. Lecomte, *Acta. Cryst. B*, to be published.
47 B. Guillot, *Acta Crystallogr., Sect. A: Found. Crystallogr.*, 2012, **68**, s204.
48 L. J. Farrugia, *J. Appl. Crystallogr.*, 1997, **30**, 565.
49 A. Volkov, T. Koristanszky and P. Coppens, *Chem. Phys. Lett.*, 2004, **391**, 170–175.
50 (*a*) G. Kresse and J. Hafner, *Phys. Rev. B: Condens. Matter Mater. Phys.*, 1993, **47**, 558–561; (*b*) G. Kresse and J. Hafner, *Phys. Rev. B: Condens. Matter Mater. Phys.*, 1994, **49**, 14251–14269; (*c*) G. Kresse and J. Furthmüller, *Comput. Mater. Sci.*, 1996, **6**, 15–60; (*d*) G. Kresse and J. Furthmüller, *Phys. Rev. B: Condens. Matter Mater. Phys.*, 1996, **54**, 11169–11186.
51 J. P. Perdew, K. Burke and M. Ernzerhof, *Phys. Rev. Lett.*, 1996, **77**, 3865–3868.
52 (*a*) P. E. Blochl, *Phys. Rev. B: Condens. Matter Mater. Phys.*, 1994, **50**, 17953–17979; (*b*) G. Kresse and D. Joubert, *Phys. Rev. B: Condens. Matter Mater. Phys.*, 1999, **59**, 1758–1775.
53 S. Grimme, *J. Comput. Chem.*, 2006, **27**, 1787–1799.
54 M. J. Frisch, G. W. Trucks, H. B. Schlegel, G. E. Scuseria, M. A. Robb, J. R. Cheeseman, G. Scalmani, V. Barone, B. Mennucci, G. A. Petersson, H. Nakatsuji, M. Caricato, X. Li, H. P. Hratchian, A. F. Izmaylov, J. Bloino, G. Zheng, J. L. Sonnenberg, M. Hada, M. Ehara, K. Toyota, R. Fukuda, J. Hasegawa, M. Ishida, T. Nakajima, Y. Honda, O. Kitao, H. Nakai, T. Vreven, J. A. Montgomery, J. E. Peralta, F. Ogliaro, M. Bearpark, J. J. Heyd, E. Brothers, K. N. Kudin, V. N. Staroverov, R. Kobayashi, J. Normand, K. Raghavachari, A. Rendell, J. C. Burant, S. S. Iyengar, J. Tomasi, M. Cossi, N. Rega, J. M. Millam, M. Klene, J. E. Knox, J. B. Cross, V. Bakken, C. Adamo, J. Jaramillo, R. Gomperts, R. E. Stratmann, O. Yazyev, A. J. Austin, R. Cammi, C. Pomelli, J. W. Ochterski, R. L. Martin, K. Morokuma, V. G. Zakrzewski, G. A. Voth, P. Salvador, J. J. Dannenberg, S. Dapprich, A. D. Daniels, O. Farkas, J. B. Foresman, J. V. Ortiz, J. Cioslowski and D. J. Fox, *Gaussian 09, Revision A.02*, Gaussian, Inc., Wallingford, CT, 2009.
55 (*a*) A. D. Becke, *J. Chem. Phys.*, 1993, **98**, 5648–5652; (*b*) C. Lee, W. Yang and R. G. Parr, *Phys. Rev. B: Condens. Matter Mater. Phys.*, 1988, **37**, 785–789.
56 Y. Zhao and D. G. Truhlar, *Theor. Chem. Acc.*, 2008, **120**, 215–241.
57 (*a*) C. Møller and M. S. Plesset, *Phys. Rev.*, 1934, **46**, 618–622; (*b*) M. Head-Gordon, J. A. Pople and M. J. Frisch, *Chem. Phys. Lett.*, 1988, **153**, 503–506.
58 R. Dovesi, V. R. Saunders, C. Roetti, R. Orlando, C. M. Zocovich-Wilson, F. Pascale, B. Civalleri, K. Doll, N. M. Harrison, I. J. Bush, P. D'Arco and M. Llunell, *CRYSTAL-09 User's Manual*, University of Turin, Turin, 2009.
59 P. Hohenberg and W. Kohn, *Phys. Rev.*, 1964, **136**, 864–871.

60 C. Lee, W. Yang and R. G. Parr, *Phys. Rev. B: Condens. Matter Mater. Phys.*, 1988, **37**, 785–789.
61 P. C. Hariharan and J. A. Pople, *Theor. Chim. Acta*, 1973, **28**, 213–222.
62 M. F. Peintinger, D. Vilela Oliveira and T. Bredow, *J. Comput. Chem.*, 2012, **34**, 451–459.
63 Y. Le Page and E. J. Gabe, *J. Appl. Crystallogr.*, 1979, **12**, 464–466.